System Design & Assessment Note

Note 45

July 2015

Experimental comparison of mode-stirrer geometries based on the susceptibility testing of COTS Information Systems in regards of the criticality of effects – Technical report – Part I

V. Houchouas, C. Kasmi, J. Lopes-Esteves, D. Coiffard

French Network and Information Security Agency, 75 007 Paris, France

name.familyname@ssi.gouv.fr

Abstract— During the last decades, the EMC/EMI community has shown a high interest in the use of reverberating chambers for the immunity testing of electronic devices. Standards have been published so that the compliance of test facilities can be checked. One of the remaining open questions is the efficiency of a mode-stirrer depending on the used material, its shape and its location within the cavity. In this paper, a description of the three main geometries encountered in the literature is given. A practical comparison of the mode-stirrers is proposed based on the Pearson correlation coefficient, the electric field distribution inside a tested computer and the results of the immunity testing of the temperature sensor enclosed in the computer under test.

Table of contents

List of Figures

List of tables

1. Introduction

The immunity and the emissivity testing of electronic devices used in critical infrastructures is of fundamental interest to define adequate protections to be inserted in the facilities in order to improve the availability of services provided to users and the confidentiality and the integrity of the processed data. The hardening of sensitive infrastructures allows for preventing threats of information leakage through spurious compromising emanations and services resilience against intentional electromagnetic interference (IEMI).

In order to characterize devices immunity, one can consider the possible electromagnetic (EM) attack scenarios and apply an EM field with well-known magnitude, direction and polarization on the target by either moving the device under test (DUT) or the source in anechoic chambers. The EMC community has shown a high interest for reverberation chambers (RC) for performing radiated immunity tests. This kind of facility constitutes another way for performing immunity testing where the DUT is placed in a fixed position in a so-called working volume (WV). For overmoded RC equipped with a moving mode-stirrer, the statistic of the field amplitude is supposed to be uniform in the WV. Thus, a quick statistic estimation of the susceptibility of the DUT can be performed.

One of the remaining open questions, as far as we know, is the definition of an efficient geometry of the mode-stirrer for a given facility. In this study, a large review of published academic and technical papers as well as pictures available on the web has been conducted. Considering, the most commonly used geometries; it has been decided to design and build the three most used mode-stirrers and to compare their stirring efficiency for a given Faraday cage thanks to the statistical tools recommended by standards. A comparison of the stirring efficiency is proposed in this paper.

During the last four years, we have been working on the susceptibility testing of information systems when exposed to parasitic field. A health monitoring software was proposed in [1] to record and characterize the effects of IEMI on a DUT by analysing drivers and operating system logs, in real-time as well as enclosed sensors. For comparison purposes, the presented software has been used in order to have a clue on the benefit of the three mode-stirrers on the criticality level of the induced perturbations for a given observable.
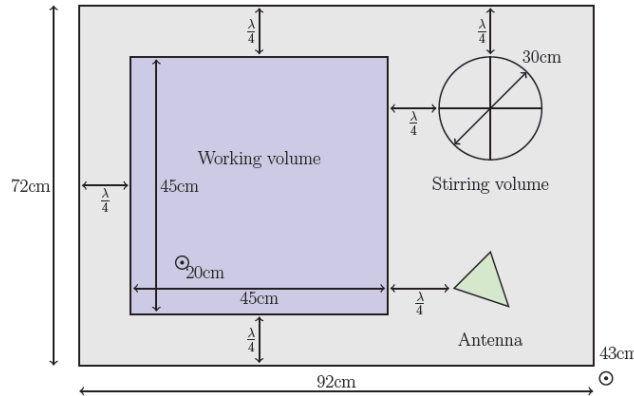

Figure 1: Schematic representing the RC.

The paper is organized as follows: in Section 2, the procedure for characterizing the efficiency of mode-stirrers in reverberation chambers is summarized. In Section 3, the benefits of the immunity testing of a commercial-off-the-shelf (COTS) computer using the mode-stirrers is discussed.

2.   Analysis of mode-stirrers

The aim of mode-stirring is to produce inside a RC a statistically uniform electromagnetic field in terms of field homogeneity and isotropy [2]. This property directly depends on the number of significantly excited modes (bounded to the mode density at the considered frequency of operation), their quality factor Q (often estimated as a composite Q factor) which quantifies the amount of energy stored in the RC, their bandwidth $BW_Q=f/Q$ and finally the stirred efficiency r_N. In this study, we only focus on the stirring efficiency parameter related to the mode-stirrer geometry.

While setting up a RC with a mode-stirrer, one has to choose its shape. Unfortunately there is no theoretical foundation, but only general guidelines [3], which provide an optimal geometry for an adequate stirring efficiency. First of all we determine the location and the maximum dimensions of the stirring volume given a required working volume (a computer 45.3 cm x 20.3 cm x 45.7 cm in what follows) in the RC. The RC we are working with is 43 cm high, 72 cm wide and 92 cm long.

The lowest usable frequency LUF as defined by [3] is included within the following range

$$LUF \in [3\ f_{TE011},\ 7\ f_{TE011}], \tag{1}$$

In our case, the LUF is:

$$LUF \in [794\ MHz,\ 1.85\ GHz]. \tag{2}$$

Another estimation from [4] links the LUF to the volume V of the RC as follows:

$$LUF = c(90/(4\pi V))^{1/3} = 879\ MHz. \tag{3}$$

Based our preliminary results [1], we have seen that interesting effects at motherboard level occur for frequencies above 2 GHz. Therefore we fixed the lowest frequency of operation $f_{MIN} = 2$ GHz (which corresponds to a maximum wavelength $\lambda_{MAX} = 15$ cm), i.e. well above these estimations of the LUF.

Moreover, it is commonly admitted that the working volume must be $\lambda_{MAX}/4 = 3.75$ cm apart from the enclosure walls and apart from the emitting antenna to ensure a uniform distribution of the field around the DUT. Finally we obtain the stirrer's volume which is a 30 cm diameter cylinder with an overall height of 34 cm. This volume must be invariant by rotation around the axis of the stirrer due to the stirrer rotation. The environment (Fig. 1) is composed of a working volume, a stirring volume and an excitation volume represented by the log-periodic antenna on Fig. 1.

2.1   Review of the proposed geometries

To find the adequate shape of the mode-stirrer one can simulate different shapes [5-7], or design a stirrer by trial and error, minimising the symmetries and then choose the more appropriate, based on their characterization. Due to the large open literature on RCs and mode-stirrers, it is also possible to rely on the existing shapes. In this work, it has been decided to select shapes from a review of commonly chosen ones in the literature (see for example [2, 7, 8, 9]). The three shapes (quoted as *S1*, *S2* then *S3*) depicted in Fig. 2 have been selected from an analysis of more than 200 references. Note that even though we selected common stirrer shapes, this does not ensure that those are the most efficient ones.

2.2 Stirring efficiency of the selected shapes

The stirred efficiency is commonly [9, 3] characterised by the Pearson correlation coefficient defined as:

$$r_N = \frac{1}{N\sigma_X^2}\sum_{i=1}^{N}(x_i - \mu_X)(y_i - \mu_Y),\qquad(4)$$

where $X = [x_0,..., x_{N-1}]$ is a series of measurements at a fixed frequency, for N consecutive mode-stirrer positions. Y is the same series rotated from one position i.e.: $Y = [x_{N-1}, x_0,..., x_{N-2}]$. μ_x is the X series mean.

In our case, X is a series of magnitude of scattering parameters $|S_{21}|$ measurements between ports 1 and 2 of a vector network analyser (VNA) connected to the 2 antennas one in the excitation volume and one in the working volume. r_N reveals the capacity of the stirrer to lead to a non-correlated field distribution in the RC for different stirrer positions. A high number of positions N is likely to create highly correlated distributions, as the angle between two positions is small. According to [3], for uncorrelated data the estimated r_N should be lower than a threshold ρ ($\rho = 1/e \approx 0.37$ for N = 30). This assumption is not relevant for N ≠ 30 as highlighted in [10].
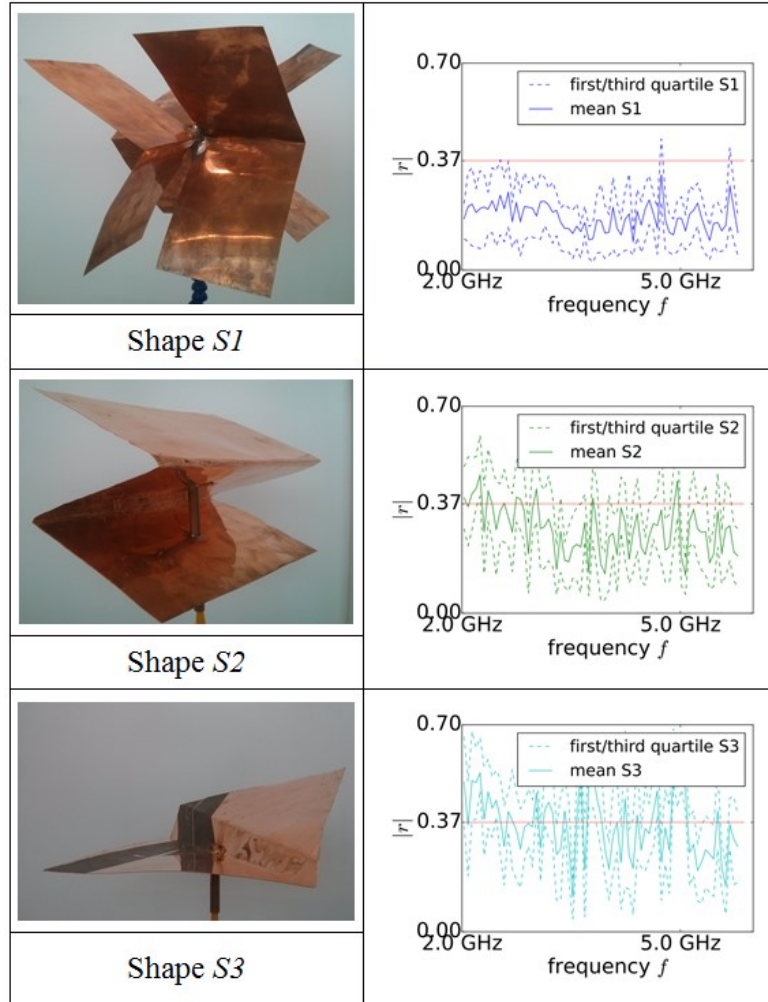

Figure 2: Picture of the three selected and designed mode-stirrers and the computed stirring efficiency using equation (4).

The stirring efficiency of each tested mode-stirrer shape is depicted in Fig. 2. The transmission parameter $|S_{21}|$ is aggregated along a full rotation of the stirrer with N = 30 steps in a bandwidth of [2 GHz, 6 GHz] with a resolution of 150 kHz using a VNA. A resolution bandwidth slightly greater than the BW_Q has been chosen while minimizing the noise floor. For graph readability, the mean, the first and the third quartiles have been estimated from the obtained r_N on blocks of 300 consecutive points of frequency.

As shown by Fig. 2, the ranking based on r_N of mode-stirrers is: *S1*, *S2* then *S3*. According to this autocorrelation function criterion *S1* appears to be much more efficient than the two others as its associated r_N is (mostly) below the threshold ρ. For shapes *S2* and *S3*, it can be mentioned that r_N decreases when the frequency increases at least in the half lower bandwidth under investigation, unlike *S1* which seems to be less sensitive to the working wavelength. This tends to prove that this stirrer provides uncorrelated realizations almost all over the considered bandwidth.

2.3 Analysis of the field uniformity in the working volume

The use of a mode-stirrer allows for generating the field uniformity in the working volume when the reverberation chamber has been well designed. The field uniformity can be validated thanks to [3]:

$$\sigma_{24}(dB) = 20 \log \left(\frac{\sigma_{24,xyz} + \langle E_{xyz} \rangle_{24}}{\langle E_{xyz} \rangle_{24}} \right), \tag{5}$$

where $< . >$ refers to the mean operator.

In order to have a clue on the field in the WV for the three designed mode-stirrers, a three-axis electric-field probe was placed in the 8 corners of the WV. The electric field magnitude was measured along the three axes while each mode-stirrer was rotating along its y-axis for 30 positions. Then, the maximum of the field amplitude along each axis were selected from the dataset to obtain 24 maximums. Then, the standard deviation of the maximums is computed using equation 5. A low $\sigma_{24}(dB)$ value means that maximums values are uniform in the WV. A threshold value of 3 dB is provided by the IEC 61000-4-21.

Table 1: Field uniformity estimator for the three mode-stirrers at the three tested frequencies.

f (GHz)	σ_{24} (dB)		
	S1	*S2*	*S3*
2	2.12	1.77	2.03
3.5	1.33	1.85	1.89
5	1.51	1.84	1.34

The field uniformity was measured for a set of frequencies and for the three geometries. It can be observed that the three shapes inside the RC allow for stimulating a uniform field in the working volume since the computed field uniformity estimator is below the standard limit of 3 dB. Nevertheless, the number of tested frequencies will be increased in the near future to enhance this study.

2.4 Analysis of the field amplitude statistic in the working volume

Many studies were devoted to the analysis of the field distribution in the working volume of a reverberation chamber. It has been demonstrated [10] that for a RC the field amplitude can be modelled with a Weibull distribution ($f_{Weibull}$). Moreover, it has been shown [10] that the field amplitude distribution depends on the wavelength. For a well dimensioned reverberation chamber, the field amplitude distribution evolves from a Weibull distribution (equation 6) for wavelengths close to the LUF, to a Rayleigh distribution (equation 7).

The Weibull probability density function is given by:

$$f_{Weibull}(x)_{k,\lambda} = \frac{k}{\lambda}\left(\frac{x}{\lambda}\right)^{(k-1)} e^{(-x/\lambda)^k}, \tag{6}$$

where k and λ refer to the shape parameter and the scale parameter of the Weibull distribution.

The Rayleigh probability density function is given by:

$$f_{Rayleigh}(x)_\sigma = \frac{x}{\sigma^2} e^{-x^2/2\sigma^2}, \tag{7}$$

where σ refers to the scale parameter of the Rayleigh distribution.

One can notice that the Rayleigh distribution is a special case of the Weibull distribution when:

$$k = 2 \text{ and } \lambda^2 = 2\sigma^2. \tag{8}$$

We analysed the statistical distribution of the field amplitude along x, y and z for the set of frequencies. The results, depicted in Fig. 3, Fig. 4 and Fig. 5, have been compared quantitatively and qualitatively. A first analysis was made by adjusting straightforwardly the field amplitudes along the three axes for the three mode-stirrers at the three considered frequencies with a Weibull distribution. A 95% hypothesis test has been conducted with the Anderson Darling hypothesis tests to the adjusted distribution along each axis. It has been confirmed that the field amplitude distribution is likely to follow the Weibull distribution.
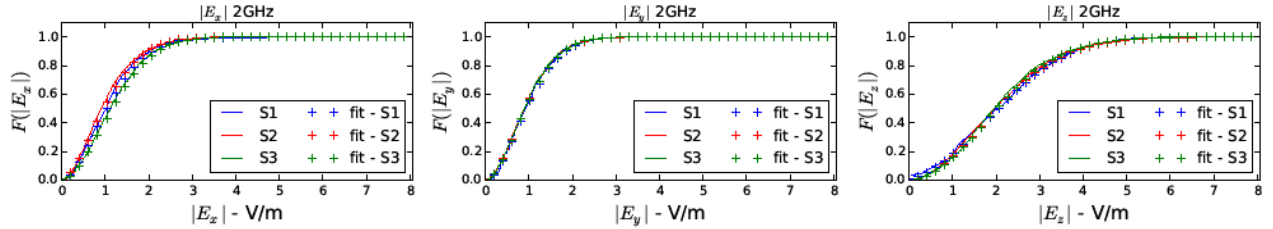

Figure 3 : Cumulative distribution function of the electric field |Ex|, |Ez| and |Ez| in the working volume at 2 GHz for the three mode-stirrers fitted with a Weibull distribution.

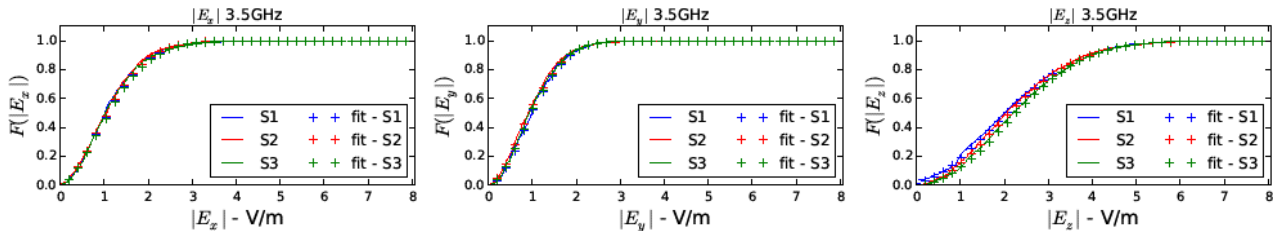**Figure 4: Cumulative distribution function of the electric field |Ex|, |Ez| and |Ez| in the working volume at 3.5 GHz for the three mode-stirrers fitted with a Weibull distribution.**
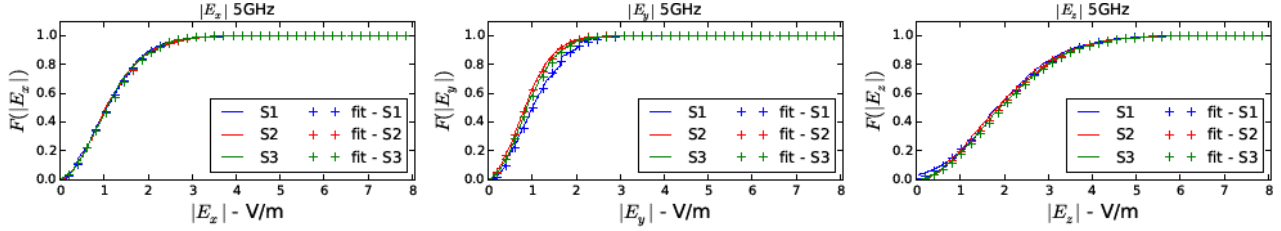
Figure 5: Cumulative distribution function of the electric field |Ex|, |Ez| and |Ez| in the working volume at 5 GHz for the three mode-stirrers fitted with a Weibull distribution.

As it was proposed in [10], the analysis has been verified by applying recursively the Anderson-Darling (AD) test to subsets of 25, 50, 75 and 150 measurements taken from the set of 1,350 ones. The subsets have been adjusted with Weibull and Rayleigh distributions thanks to the maximum log-likelihood method.

Table 2: Rejection rate of the Hypothesis that field amplitude subset (the length of the sample is 50) along the three-axis is following a Weibull or a Rayleigh distribution based on the AD test.

f (GHz)	distribution	AD tests (%)		
		S1	*S2*	*S3*
2	Weibull	11.11	11.11	14.81
	Rayleigh	14.8	11.11	7.41
3.5	Weibull	18.51	0.51	14.81
	Rayleigh	23.92	3.71	3.70
5	Weibull	8.23	3.74	7.41
	Rayleigh	9.55	3.79	7.41

Using the Anderson-Darling hypothesis test, the rejection rates of the hypothesis are provided in Table 2 for subsets of 50 values. Again it can be observed that the three selected shapes, the reverberation chamber seems to stimulate very similar field amplitude distributions. Nevertheless, the number of frequencies should be increased to confirm these results.

3. Immunity testing of electronic device

To evaluate the immunity of an information system, different techniques can be applied. One can either measure the field inside a computer, or induced voltages in circuits, or record the number of faults on a running system. In this Section, the penetration of the electric field through apertures at three points of interest in the computer is analysed. Then, a brief overview of observable faults induced on the computer by parasitic fields is presented. According to previous experiments [1], it has been observed that around 2 GHz the temperature sensor is highly susceptible. In this section, we will focus on this working frequency and this observable to compare the mode-stirrer shapes based on the criticality of the induced effects [11].

3.1 Mode-stirrers classification thanks to the induced electric field

The three positions, depicted in Fig. 6, are of high interest as susceptible components [1] are placed in these parts of the computer (P1: hard-disk drive, P2: PCI slots and P3: CPU cooling fan). In order to analyse the contribution of the different mode-stirrers, the distribution of the electric field along x, y and z in the computer has been compared for the three mode-stirrers. The three components ($|Ex|$, $|Ez|$ and $|Ez|$) of the electric field induced in the computer cavity have been measured at the three positions for a set of

frequencies. Boxplot representations of the field values for three mode-stirrers are proposed in Fig. 7. It can be observed that for the three positions, the three mode-stirrers stimulate the field amplitude mean contributions along the three axes similarly. At the position 1, the component |Ex| is more widely distributed than the two others components. Moreover, some outliers (represented by blue crosses) can be observed at the position 3 which is of high interest in our case as the temperature sensor is next to the CPU Cooling fan.
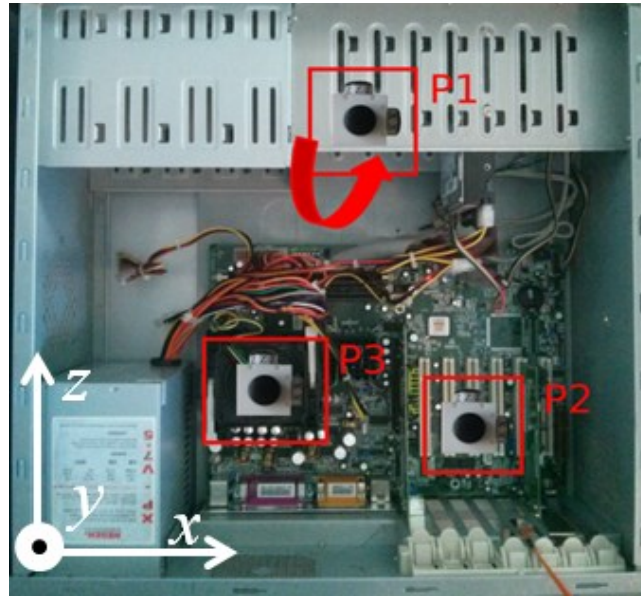

Figure 6: Electric field probe inside the computer box at the three chosen positions [11].

3.2 Mode-stirrers classification based on faults severity

Linux has been installed on the computer in order to gain easy access to drivers and operating system logs. Faults [1] (ex. USB, PS2 and temperature sensors) induced by IEMI can be detected. The computer was tested using the described approach and it has been observed that the I7 CPU clock balancing was highly deteriorated. Moreover, it has been observed that the effects (ex. clock balancing deterioration, temperature sensors errors) were induced at different levels of criticality depending on the mode-stirrer and the frequency.
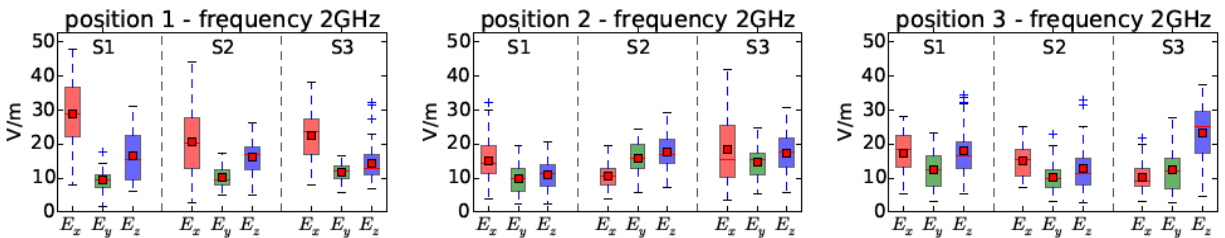

Figure 7: Boxplot representation of the electric field measured inside the computer box at the positions 1, 2 and 3 for a working frequency of 2 GHz [11].

As for an example, we propose to sum up a comparison of the perturbations of the communication links between the temperature sensor and the CPU for a full rotation of each mode-stirrer considering a fixed power level on the signal generator (EM field strength) [11]. As we considered the temperature sensor reading errors, highlighted in Fig. 8 [1], we focus on the field statistics at the position 3 above the CPU of the motherboard cooling fan where the sensor is located. It has been pointed out that the field amplitude

along z seems to be identically excited by three mode-stirrers. The field amplitude along x is better stimulated by the mode-stirrers *S1* and *S2*. The field amplitude along y is better stimulated by shapes *S1* and *S3*. The ranking based on the field amplitude stimulation is: *S1-S2-S3* along x, *S3-S1-S2* along y and *S3-S2-S1* along z.

The recorded temperature can be modified by two factors:

-   The temperature in the RC increases due to a lack of cooling and the CPU activity;

-   The parasitic coupling on the printed circuit board (PCB) that disturbs the communication between the sensor and the CPU. It has been shown in [1] that the level of the reported temperature increases with the generated parasitic field strength.
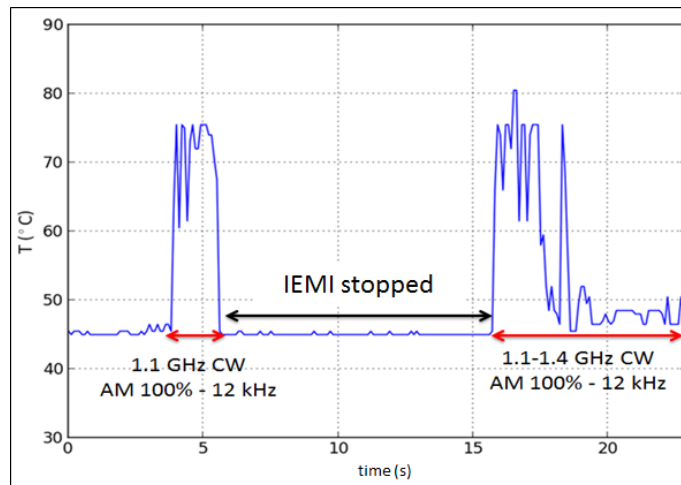

Figure 8: Estimation of the resonating frequency of the temperature sensor for EM coupling maximization [1].

In the preliminary experiments, the temperatures during normal activity have been recorded. It has been observed that the temperature slowly grows from $T_{t_i}= 45°C$ to $T_{t_f} =48°C$. Then, the temperature is measured when activating the EM generator (a 2 GHz continuous wave for a given temperature) and the mode-stirrers. The induced reading errors of the temperature are proposed in Fig. 9. It can be pointed out that the mode-stirrer *S1* allows for inducing the highest criticality effects. This conclusion is directly linked to the stirring efficiency of *S1*. Indeed, *S1* is capable to set different field topologies up in the computer.
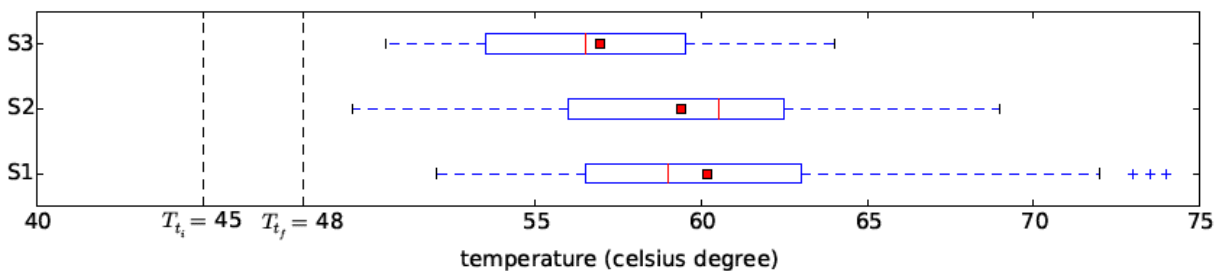

Figure 9: Boxplot of the temperature sensors erroneous measurement due to a 2 GHz continuous wave for a complete rotation of each mode-stirrer [11].

Different field topologies involve different EM to PCB coupling configurations. The reported temperature reading error is widely distributed in regards to the shape *S1*. On the contrary, the mode-stirrers *S2* and *S3* induce low criticality errors (due to lower stirring efficiency). Nevertheless, it can be observed that the mean contributions (highlighted by the mean in red point and the median represented by the red line in Fig. 9) of the induced errors are very similar. The induced reading errors of the temperature are shown in Fig. 9 for a complete rotation of the mode-stirrers. The related boxplot for each reading errors distribution is proposed. The highest is the measured temperature the highest is the criticality of the effect. It can be pointed out that mean contributions of errors are very similar when using shapes *S1* and *S2*. Outliers can be observed only when using *S1*. The severity of reading errors is lower for *S3* than for *S1* and *S2* (the ranking based on the severity dynamics of effects over one full rotation of the mode-stirrers is *S1*, *S2* and *S3*). Based on the ranking of mode-stirrers and based on the severity analysis of effects and the field excitation in the computer box, it has been assessed that the parasitic coupling is mostly due to the field component along *x*.

4.   Conclusion

An exhaustive review of mode-stirrers geometry has been performed leading to the study of more than 100 conference and journal papers, 25 PhD theses and a large number of pictures available on the Internet. The three most common shapes have been designed and tested in order to have a clue on their stirring efficiency for a given reverberating chamber. The following aspects have been investigated to compare the designed geometries:

- The main lines of standardized tests have been performed, namely: the Pearson correlation parameter for estimating the so-called stirring efficiency related to the samples correlation, the characterization of the field uniformity in the working volume and the statistical analysis of the field amplitude. It has been observed that even for non-negligible correlation parameters, the uniformity of the field and the field amplitude for the three shapes are good enough;

- Once the RC has been designed, its use for characterizing the susceptibility of a computer has been studied. First, the field penetration in a computer box through its apertures has been statistically analysed for the three geometries. It has been observed that the designed mode-stirrers allow for well stimulating the field penetration. Based on the working frequency and the position in the computer, it has been observed that the mode-stirrers have more or less equivalent performances;

- The correlation between field penetration through apertures and detected/recorded effects induced by parasitic field on the computer has been studied. We focused on the communication between the temperature sensor and the CPU which is highly susceptible to parasitic fields. The criticality of errors for each mode-stirrer has shown that the mode-stirrer *S1* (which is the shape giving the best performances based on standardized tests) allows for stimulating a large number of field topologies.

In this paper, it has been confirmed that the reverberation chamber provides interesting outcomes in the characterisation of the susceptibility of electronic devices to IEMI. Moreover, it has been observed that the choice of the mode-stirrer shape is crucial as the type of effects and their criticality is highly related to this factor for a given emitted field strength.

5. Futur work and remarks

Further work will be dedicated to use statistical observables for comparing the mode-stirrer geometries performance when changing the position of the stirrer in the RC. Moreover, more devices will be tested. The type and the criticality (e.g. DRAM errors, Cooling fan speed) of effects will be involved for analysing the stirring efficiency of selected shapes.

Moreover, the study presented in this paper raised interesting discussions with reviewers concerning the mode density excited in the reverberation chamber. While the results are considered as correct, in the near future, the authors will work on the characterization of the mode density and the quaity factor of the small chamber presented in this study. Moreover, the defined lowest usable frequency has been estimated thanks to standards related to room sized chambers. Part of the work will be dedicated to the analysis of the pertinence of the presented approach for the definition of the lowest usable frequency. It can be mentioned that small size testing chambers are of fundamental interests as they allow for analyzing the susceptibility of electronic devices enclosed in small cavities like avionic bay [12]. The results of the forthcoming work will be submitted in a following System Design and Assessment Note as a "Technical report – Part II".

References

[1] C. Kasmi, J. Lopes Esteves, M. Renard, "Automation of the immunity testing of COTS computers by the instrumentation of the internal sensors and involving the operating system logs - technical report". *System Design and assessment Note* 44, Nov. 2014.

[2] J.-I. Hong and C.-S. Huh, "Optimization of stirrer with various parameters in reverberation chamber". *Progress In Electromagnetics Research*, 104:15-30, 2010.

[3] IEC 61000-4-21, Electromagnetic Compatibility (EMC) — Part 4-21: Testing and Measurement Techniques Reverberation Chamber Test Methods, 2003.

[4] IEEE 299.1, IEEE standard method for measuring the shielding effectiveness of enclosures and boxes having all dimensions between 0.1 m and 2 m. 2013.

[5] K. Selemani, J.-B. Gros, E. Richalot, et al. "Comparison of reverberation chamber shapes inspired from chaotic cavities". *IEEE Transactions on EMC*, 2014.

[6] J.-S. Kim, R. Mittra, "Numerical study of stirring effects in a mode-stirred reverberation chamber by using the finite difference time domain simulation". *Forum for Electromagnetic Research Methods and Application Technologies* (FERMAT).

[7] J. Clegg, A. Marvin, J. Dawson, et al, "Optimization of stirrer designs in a reverberation chamber". *IEEE Transactions on EMC*, 47(4):824-832, Nov. 2005.

[8] Y. Huang, N. Abumustafa, Q. Wang, et al, "Comparison of two stirrer designs for a new reverberation chamber". In *Environmental Electromagnetics, The 2006 4th Asia-Pacific Conference*, pp. 450-453, Aug., 2006.

[9] N. Wellander, O. Lundén, M. Bäckström, "Experimental Investigation and Mathematical Modeling of Design Parameters for Efficient Stirrers in Mode Stirred Reverberation Chambers", *IEEE Transactions on EMC*, Vol. 49, No. 1, pp. 94 – 103, February 2007.

[10] C. Lemoine, *"*Contribution to the statistical analysis of measurements data in mode-stirred reverberation chamber" – "Applications for the evaluation of stirring efficiency and measurements uncertainty in the context of radiofrequencies and EMC". Ph.D. Thesis*,* INSA*, Rennes,* Jul. 2008.

[11] V. Houchouas, C. Kasmi, J. Lopes Esteves, D. Coiffard: "Analysis of effects induced by parasitic fields on electronic devices in reverberation chambers: comparison of the performances of three mode-stirrers". Electronics Letters, under review, July, 2015.

[12] B. Vallhagen, C. Samuelsson, M Bäckström, "Determination of Q-value of an Avionics Bay or Other Multiresonant Cavity by Measurements in Time- and Frequency-Domain, with One or Two Antennas", In Proc. of ASIAEM 2015, Jeju, South-Korea, August 2015.